Low-insertion-loss Gysel power combiner with high power density and high isolation

Song Guo [iD], Kaijun Song and Yong Fan

EHF Key Lab of Fundamental Science, School of Electronic Science and Engineering, University of Electronic Science and Technology of China, Chengdu 611731, China

Abstract

A suspended-stripline Gysel low-insertion-loss power combiner is presented in this paper. The multi-layer cavity structure reduces the circuit size and increases power density, composed of suspended strip lines and coaxial lines. The transmission-line theory is used to analyze this proposed power combiner, and the equivalent circuit model is developed to investigate the characteristics and design of the power combiner. The measured input return loss is greater than 20 dB from 7.15 to 9.35 GHz. The measured insertion loss is less than 0.36 dB, and the power-combining efficiency is greater than 92% from 7.39 to 9.19 GHz. The maximum power-combining efficiency is 98.8% at 8.1 GHz. Besides, the measured isolation is greater than 20 dB from 7 to 10 GHz. The power capacity is analyzed, and the cross-sectional power density is greater than $3.57\,\text{kW/cm}^2$. The measured and simulated results show reasonable agreement with each other.

Introduction

Power combiners and dividers have various radar systems applications, such as power-combining amplifiers and antenna arrays [1–16]. Many researchers have proposed solutions to the joint design of compactness, low loss, high isolation, and high power density. Several waveguide power dividers with low insertion loss have been intensively investigated [2, 8, 17]. However, they suffer from large size and cannot meet the demands of high isolation with wide bandwidth. On the other hand, the power dividers designed with microstrip lines [3, 18, 4–6, 11, 9, 13] show the potential of compact size and easy integration with active devices compared with waveguide power dividers. In [3], a two-way balanced Gysel power divider with wide bandwidth is proposed to modify the standard five-port divider. In [4, 5], Gysel power dividers with arbitrary power division ratios have been studied. Nevertheless, they are not suitable for high power combination with low loss. In [19], suspended stripline with high power-handling capacity is applied to reduce the loss. However, isolation is not high enough. In the previous work [16], a suspended-stripline power divider is designed. The required isolations among the output ports are obtained by connecting floating embedded resistors in its circuit configuration. Nevertheless, these resistors are damaged easily because of missing heat transfer provision to the ground plane when the input port's power is out of balance.

In this paper, the design and fabrication of a four-way Gysel suspended-stripline power combiner with high power-combining efficiency at the X-band are described. An equivalent circuit model is used for accurate analysis and optimization. Attractive features of low loss, high isolation, and high power density are obtained. Additionally, the proposed power combiner realizes high power-combining efficiency and high power density without significantly increasing the circuit size.

Structure, analysis, and design

The basic configuration of the proposed four-way Gysel power combiner is shown in Fig. 1. The proposed power combiner is composed of the power-combining network and the isolation network. Suspended stripline has been used in the power-combining circuit and the insolation circuit. Air-filled coaxial lines are applied to connect the suspended-stripline power-combining circuit. One end of the inner conductor is connected to the suspended-stripline power-combining circuit through substrate 2. The connection nodes are A′ (as denoted in Fig. 1(c)). The other end is connected to the other insolation circuit through substrate 1. The connection nodes are C′ (shown in Fig. 1(a)). Four cylindrical high-power isolation resistors are located on the nodes C′, while the other ends of the resistors are soldered to the upper cavity.

Since the proposed power combiner can be viewed as a symmetric structure, it can be analyzed by applying the even- and odd-mode equivalent-circuit method, as shown in Fig. 2. The odd-mode and even-mode equivalent circuits are shown in (Figs 2(b) and 2(c)), respectively.
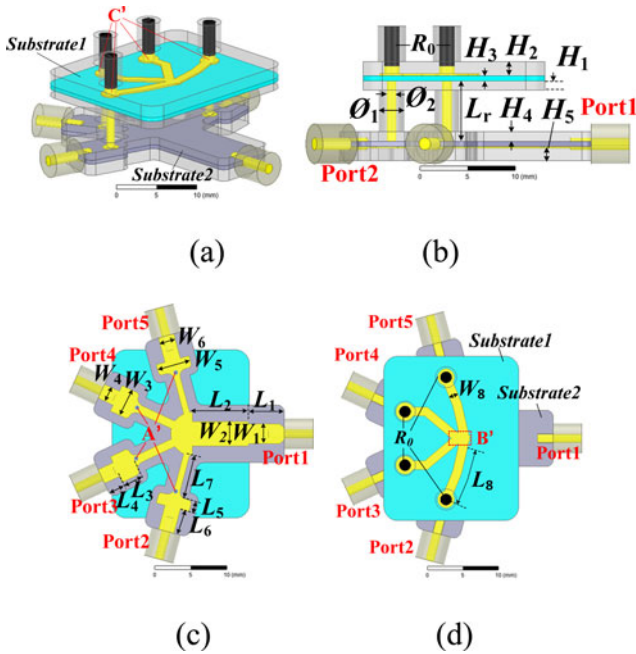
Fig. 1. Proposed suspended-stripline power combiner: (a) 3D view, (b) Side view, (c) Bottom view of substrate 2, (d) Top view.

The analysis method can also be applied to analyze unequal power division networks. The lines with wide width result in a large capacitance at the common point, leading to circuit mismatch. As shown in Fig. 1(d), the common point B′ of the isolation network introduces lumped capacitance C_1 in the equivariant circuit. As shown in Fig. 1(c), the connection point A′ of the air-filled coaxial line and the power-combining network introduce capacitances C_2. The coaxial line of length L_r is equated to an ideal transmission line of impedance Z_{vj} and electrical length θ_v. The ratio of the output power P_0 to the input power P_j of the jth port is $P_0/P_j = K_j$. K_j satisfies as follows:

$$\sum_{j=2}^{N+1}(1/K_j) = 1 \qquad (1)$$

K_j can be calculated by the actual power division ratio, so the output impedance Z_{oj} of each way is as follows:

$$Z_{oj} = K_j Z_0, \ j = 2, 3, \ldots, N+1 \qquad (2)$$

Under equal power division ratio case, $K_j = N$. When odd-mode excitation is applied, the jth port is excited with power P_j, and the sum of the powers excited at the other $N-1$ input ports is $P_{sumN-1} = (K_j - 1)P_j$. The voltage at the jth input port is 180° out of phase with the voltage at the $N-1$ input ports. In this case, node B′ is equated to an electrical wall. The corresponding input impedances of Z_{1j}^o and Z_{2j}^o in Fig. 2(b) are as follows:

$$Z_{1j}^o = jR_{0j}Z_{uj}\tan\theta_{uj}/(jZ_{uj}\tan\theta_{uj} + R_{0j}), \ j = 2, 3, \ldots, N+1 \qquad (3)$$

$$Z_{2j}^o = \frac{Z_{vj}(Z_{1j}^o + jZ_{vj}\tan\theta_v)}{Z_{vj} + jZ_{1j}^o\tan\theta_v}//Z_{c2j}, \ j = 2, 3, \cdots, N+1 \qquad (4)$$

where $Z_{c2j} = 1/j\omega C_{2j}$, ω is the operating frequency. Then the odd-mode input reflection coefficient Γ_{1j}^o can be characterized as follows:

$$\Gamma_{1j}^o = \frac{-Z_0 Z_i^o + j(Z_i^o Z_{tj} - Z_0 Z_{tj})\tan\theta_t}{Z_i^o Z_0 + j(Z_i^o Z_{tj} + Z_0 Z_{tj})\tan\theta_t}, \ j = 2, 3, \ldots, N+1 \qquad (5)$$

Similarly, when even-mode excitation is applied, node B′ is equated to an electrical wall. The input impedances Z_{1j}^e and Z_{2j}^e in Fig. 2(c) can be obtained as follows:

$$Z_{1j}^e = \frac{Z_{uj}(Z_{c1} + jZ_{uj}\tan\theta_{uj})}{jZ_{c1}\tan\theta_{uj} + Z_{uj}}//R_{0j}, \ j = 2, 3, \ldots, N+1 \qquad (6)$$

$$Z_{2j}^e = \frac{Z_{vj}(Z_{1j}^e + jZ_{vj}\tan\theta_v)}{Z_{vj} + jZ_{1j}^e\tan\theta_v}//Z_{c2j}, \ j = 2, 3, \ldots N+1 \qquad (7)$$

where $Z_{c1j} = 1/j\omega C_j$ and $Z_{c2j} = 1/j\omega C_{2j}$. C_{1j} is satisfied as follows:

$$\sum_{i=2}^{N+1} C_1 j = C_1 \qquad (8)$$

Then the even-mode input reflection coefficient Γ_{2j}^e and output reflection coefficient Γ_{1j}^e can be characterized as follows:

$$\Gamma_{1j}^e = \frac{((K_j - 1)Z_i^e - K_j Z_0)Z_{tj}Z_0 - j(K_j Z_0 Z_i^e + Z_{tj}^2 - Z_{tj}^2 Z_i^e)\tan\theta_t}{((K_j + 1)Z_i^e + K_j Z_0)Z_{tj}Z_0 + j(K_j Z_0 Z_i^e + Z_{tj}^2 + Z_{tj}^2 Z_i^e)\tan\theta_t},$$
$$j = 2, 3, \ldots, N+1,$$
$$(9)$$

$$\Gamma_{2j}^e = \frac{Z_0 Z_{tj}(Z_i^e - K_j Z_i^e - K_j Z_0) + j(Z_{tj}^2 Z_i^e + Z_{tj}^2 Z_0 - K_j Z_i^e Z_0^2)\tan\theta_t}{Z_0 Z_{tj}(Z_i^e + K_j Z_i^e + K_j Z_0) + j(Z_{tj}^2 Z_i^e + Z_{tj}^2 Z_0 + K_j Z_i^e Z_0^2)\tan\theta_t},$$
$$j = 2, 3, \ldots, N+1.$$
$$(10)$$

Then, the value of the input reflection coefficient Γ_{inj} and output reflection coefficient Γ_{outj} can be found to be

$$\Gamma_{inj} = \frac{\Gamma_{1j}^o + \Gamma_{1j}^e}{2}, \ j = 2, 3, \ldots, N+1, \qquad (11)$$

$$\Gamma_{outj} = \Gamma_{2j}^e, \ j = 2, 3, \ldots, N+1. \qquad (12)$$

According to equations (11) and (12), the input and output reflection coefficients under different conditions can be obtained, respectively. To simplify the calculations, always let $Z_0 = 1$. The proposed work is a four-way balanced power division network, so $K_j = 4$. There is only one transmission pole for the traditional Gysel power combiner ($Z_{uj} = Z_{vj} = 1$, $Z_t = 2$, $\theta_u = \theta_v = \theta_t = 0.5\pi$) without node capacitance. Z_t is reduced reasonably to obtain two transmission poles simultaneously for both Γ_{inj} and Γ_{outj} as shown in Fig. 3(a). Then the bandwidth of the power combiner can be broadened. As a matter of fact, the capacitances C_1 and C_{2j} cause the mismatch of the input and output reflection in practice, as
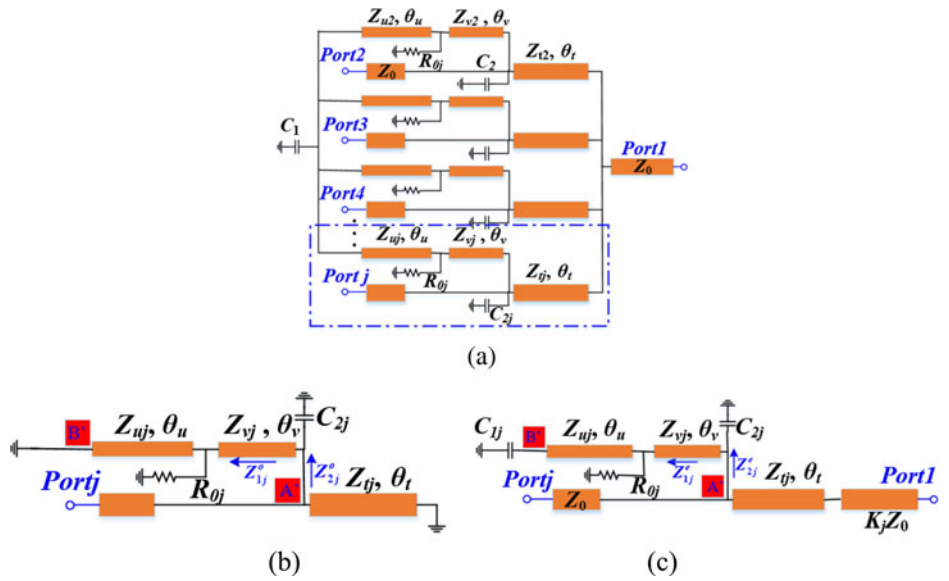
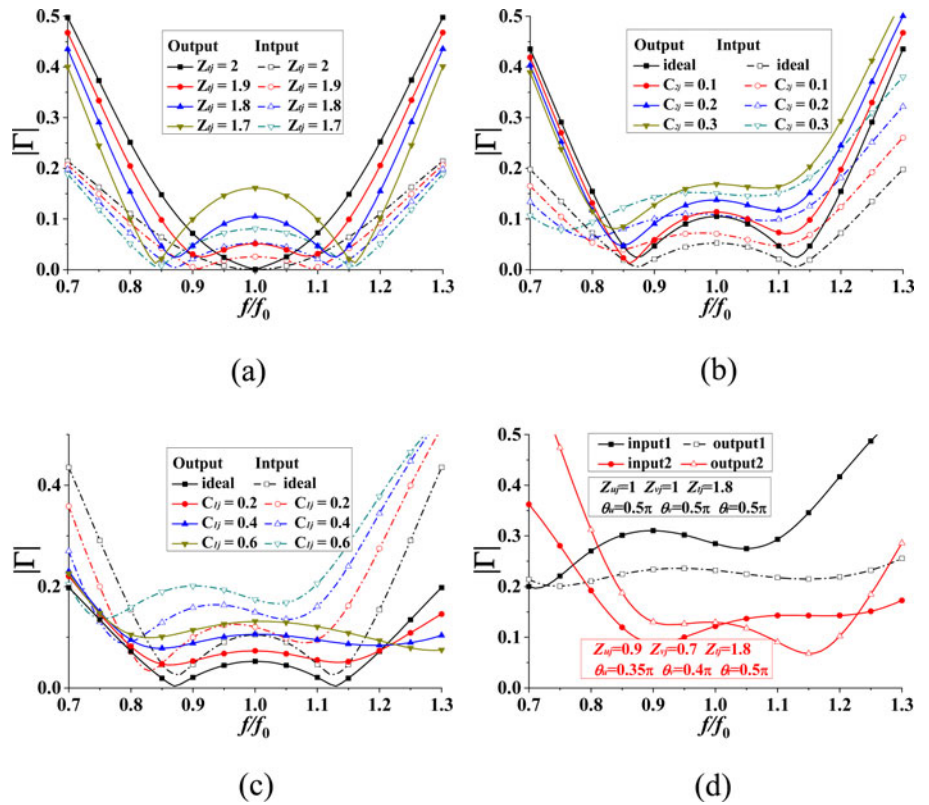**Fig. 2.** (a) Equivalent circuit model, (b) Odd mode, (c) Even mode.

Fig. 3. Input and output reflection coefficients with varied (a) Z_{tj}, (b) C_{1j}, and (c) C_{2j}, (d) The optimization of input and output reflection coefficient.
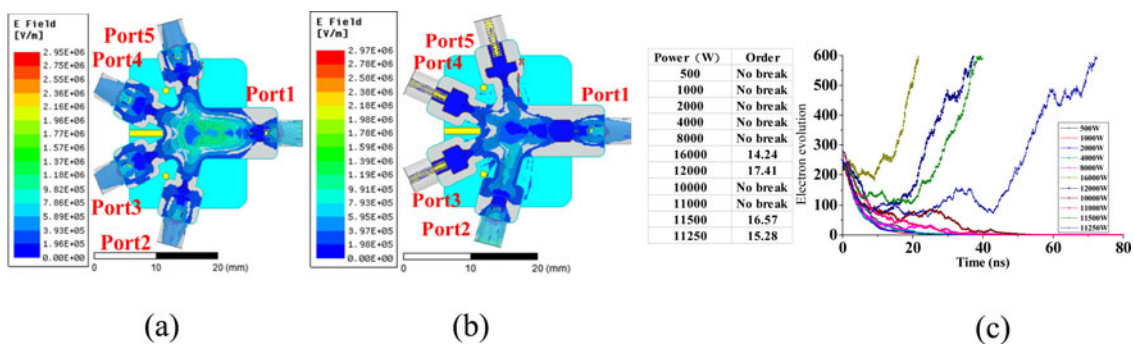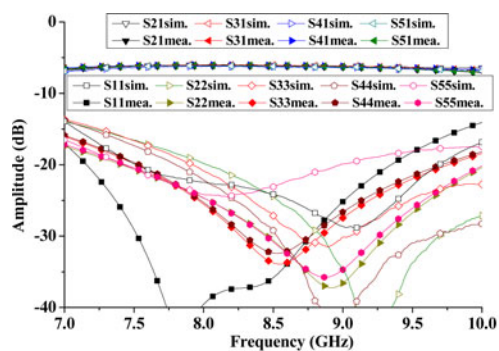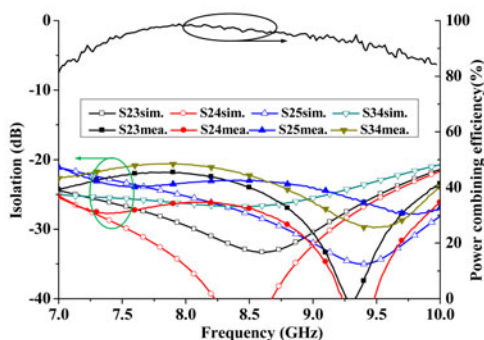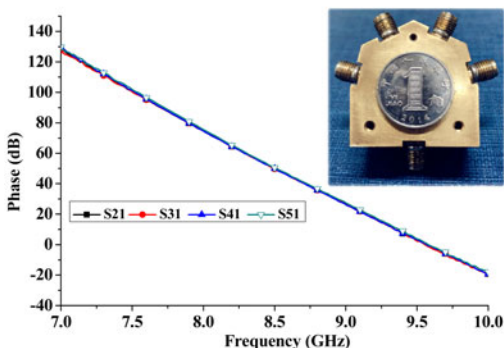

Fig. 4. Simulated electric field: (a) Input power of 25 kW from Port1, (b) Input power of 25 kW from Port2, (c) Electron evolution curve at different power.

Fig. 5. Simulated and measured results: (a) Input/Output return loss and insertion loss, (b) Isolation and power combining efficiency, (c) Measured results of phase.

shown in (Figs 3(b) and 3(c)). For odd mode, the resistor has power loss, when $\theta_u = \theta_v = 0.5\pi$, based on equations (3) and (4), Z_i^o can be made equivalent to an resistor capacitor and inductor parallel network. So the center frequency of the input reflection coefficient shifts to a lower frequency when C_{1j} and C_{2j} increase. According to equation (9), the output reflection coefficient is only determined by the even-mode circuit. Based on equations (6) and (7), when $\theta_u = \theta_v = 0.5\pi$, $Z_{2j}^e \approx 1/j\omega(mC_{1j} + C_{2j})$. m is related to Z_{uj} and Z_{vj}. As shown in (Figs 3(b) and 3(c)), the output reflection coefficient's center frequency is constant. At the same time, they are both getting worse. As shown in Fig. 3(d), the black curves show the mismatch with both node capacitances C_{1j} and C_{2j}. The red

curves Fig. 4(d) show the optimized input and output reflection coefficient. It is sufficient that Z_{ug}, Z_{vj}, θ_u, and θ_v can be reduced to achieve a better reflection coefficient.

Furthermore, the power-handling capability of the power combiner is analyzed. As shown in (Fig. 4(a) and 4(b)), when 25 kW power is applied from the power-combining port, the maximum electric field is around 2.97×10^6 V/m, which is less than the simulated breakdown electric field (3×10^6 V/m) of air. As shown in Fig. 4(c), the multipactor evolution process is simulated in Spark3D. The electron number increase for situations occurrence offers multipactor phenomenon taken place at about 11.5 kW (air critical breakdown power). The cross-sectional power density (CSPD) can be calculated as 3.57 kW/cm² by using

$$\text{CSPD} = \frac{\text{Air critical breakdown power}}{\text{Maximum cross-sectional area}} \qquad (13)$$

The maximum cross-sectional area is 2.82 cm × 1.09 cm. This power combiner can be operated at high power applications.

Results and discussion

A Gysel suspended-stripline power combiner was designed according to the analysis above. It was simulated and optimized in the full-wave simulation software HFSS. The four-way power combiner has been fabricated by machining suspended-stripline in copper blocks on the substrate Taconic RF-35 with a relative dielectric constant of 3.5, the thickness of 0.508 mm, and a loss tangent of 0.0018. The final dimensions of the proposed power divider are as follows (unit: mm): $L_1 = 4.95$, $L_2 = 7.95$, $L_7 = 6$, $L_5 = 1.57$, $L_6 = 3.42$, $L_3 = 2.72$, $L_4 = 2.3$, $L_8 = 8.91$, $W_8 = 1.29$, $W_5 = 4.72$, $W_6 = 2.2$, $W_3 = 3.9$, $W_4 = 2.1$, $W_2 = 1.29$, $W_1 = 1.88$, $\varnothing_1 = 1$, $\varnothing_2 = 2.6$, $H_1 = 0.5$, $H_2 = 0.508$, $H_3 = 1.5$. The isolation resistors are 50 Ω. A photograph of the fabricated suspended-stripline power divider is shown in Fig. 5(c), and the circuit size of the area is $0.60\lambda_g \times 0.80\lambda_g \times 0.34\lambda_g$ ($W \times L \times H$).

The fabricated power combiner has been measured by using vector network analyzer Agilent N5244A. Figure 5 shows that the measured input return loss(S_{11}) is greater than 20 dB from 7.15 to 9.35 GHz. Moreover, it is greater than 25 dB from 7.35 to 9.01 GHz. The measured output return loss(S_{nn}, $n = 23,4$) is at least 20 dB from 7.92 to 9.75 GHz. The measured insertion loss is less than 0.36 dB, and power combining efficiency is greater than 92% from 7.39 to 9.19 GHz. The maximum power-combining efficiency of 98.8% can be observed at 8.1 GHz. Meanwhile, as shown in Fig. 5(b), the measured output isolation is greater than 20 dB from 7 to 10 GHz. The measured results and the simulated ones show a reasonable agreement with each other. The difference between the simulated and measured results is partly due to machining and assembly errors, and partly to inaccuracies of the dielectric constant of the substrate.

The power-combining port's power capacity has been tested under 10 kW pulse excitation with 1‰ duty cycles. In comparison, the power-dividing ports' power capacity has been tested under 5 kW pulses, as shown in Fig. 6. The test pulse power can be transmitted through the fabricated power combiner, and the electric breakdown phenomenon and a thermal breakdown do are not generated as shown in Fig. 7. The CSPD is greater than 3.57 kW/cm². A comparison with other four-way power dividers is shown in Table 1. It can be seen that the presented Gysel power combiner has the advantages of low loss, high power-combining efficiency, relatively high isolation, high power density,
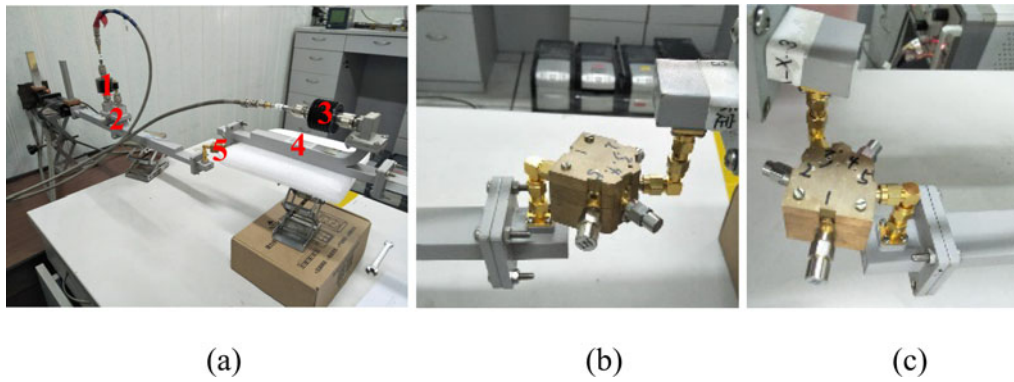
Fig. 6. (a) Scenario of power capacity testing: (b) Transmission test, (c) Isolation test.
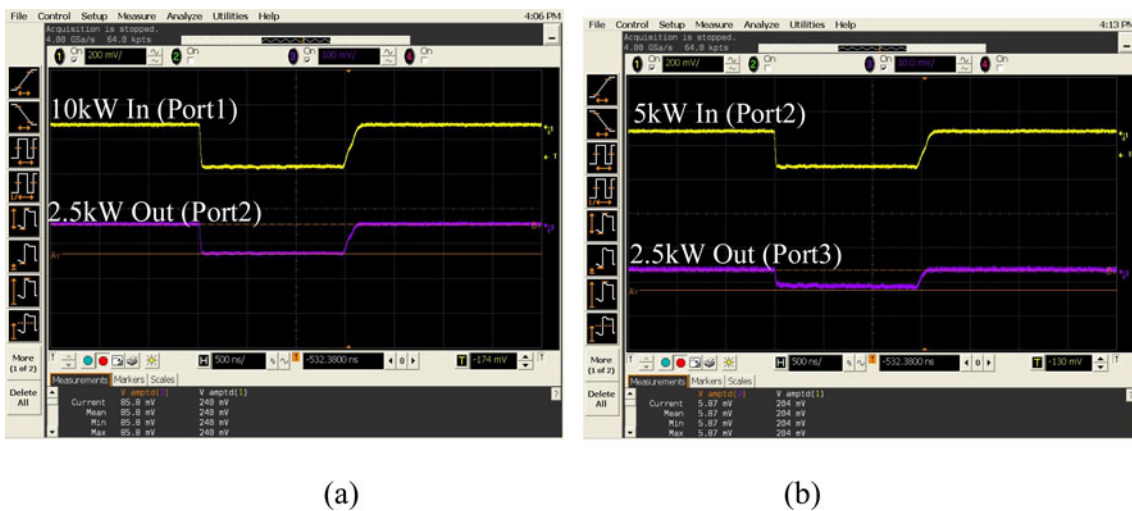

Fig. 7. Waveform of power capacity testing: (a) Transmission test, (b) Isolation test.

Table 1. Comparison between the proposed power divider and reported ones.

Works	Freq. (GHz)	IRL (dB)	ORL (dB)	Iso (dB)	Ins (dB)	PCE (%)	CSPD (kW/cm^2)	HPC
[2]	2.1–2.5	>15	—	>8	<1	79	—	—
[13]	1–1.1	>20	>18	>20	<1	79	—	—
[19]	12.1–15.7	>19	>6	>7	<1.4	72	—	—
[7]	31–38	>15	/	>10	<0.75	84	—	—
[9]	4.1–5.7	—	>14	>4	<1.5	71	—	—
[16]	7.5–9.5	>20	>20	>20	<0.37	>92	—	No
This work	7.92–9.53	>28	>20	>20	<0.37	>92	3.57	Yes

IRL, Input return loss (S_{11}); ORL, Output return loss (S_{nn}, $n = 23,4$); Iso, Isolation; Ins, Insertion loss; PCE, Power-combining efficiency; CSPD, Cross-sectional power density; HPC, High power capacity.

and good input/output impedance matching in the operating frequency band.

Conclusion

In this paper, a four-way suspended-stripline Gysel power combiner is demonstrated. The developed equivalent model has been discussed. The measured results are in good agreement with the simulated ones. The proposed four-way power combiner has low insertion loss, high power-combining efficiency, high isolation, high power density, and good input/output impedance matching. It can be used in multiway high power-combining amplifiers, antenna arrays, and mixers.

References

1. **Gysel UH** (1975) A New N-Way Power Divider/Combiner Suitable for High-Power Applications, in *1975 IEEE-MTT-S International Microwave Symposium*, pp. 116–118.
2. **Becker JP and Oudghiri AM** (2005) A planar probe double ladder waveguide power divider. *IEEE Microwave & Wireless Components Letters* **15**, 168–170.
3. **Oraizi H and Sharifi A-R** (2009) Optimum design of a wideband two-way Gysel power divider with source to load impedance matching. *IEEE Transactions on Microwave Theory and Techniques* **57**, 2238–2248.
4. **Oraizi H and Sharifi A-R** (2011) Optimum design of asymmetrical multi-section two-way power dividers with arbitrary power division and impedance matching. *IEEE Transactions on Microwave Theory and Techniques* **59**, 1478–1490.
5. **Oraizi H and Ayati S-A** (2011) Optimum design of broadband n-way rectangular power dividers with arbitrary power division and impedance matching. *IET Microwaves, Antennas & Propagation* **5**, 1447.
6. **Oraizi H and Ayati SA** (2012) Optimum design of a novel N-way planar power divider/combiner with impedance matching. *IET Microwaves, Antennas & Propagation* **6**, 418.
7. **Chu Q, Kang Z, Wu Q and Mo D** (2013) An in-phase output Ka-Band traveling-wave power divider/combiner using double ridge-waveguide couplers. *IEEE Transactions on Microwave Theory & Techniques* **61**, 3247–3253.
8. **Chu Q, Mo D and Wu Q** (2015) An isolated radial power divider via circular waveguide TE01-mode transducer. *IEEE Transactions on Microwave Theory and Techniques* **63**, 3988–3996.
9. **Song K, Hu S, Zhang F and Zhu Y** (2015) Four-way chained quasi-planar power divider using rectangular coaxial waveguide. *IEEE Microwave and Wireless Components Letters* **25**, 373–375.
10. **Li GL, Song KJ, Zhang F and Zhu Y** (2015) Novel four-Way multilayer SIW power divider with slot coupling structure. *IEEE Microwave and Wireless Components Letters* **25**, 799–801.
11. **Oraizi H and Yousefi A** (2017) Optimum design of a wideband planar N-way fork power divider with arbitrary power division and input-to-output impedance matching. *AEU - International Journal of Electronics and Communications* **79**, 83–93.
12. **Wu B, Zhang Y, Zhao Y, Zhang W and He L** (2018) Compact nine-way power divider with omnidirectional resistor based on graphene flake. *Microwave & Wireless Components Letters IEEE* **28**, 762–764.
13. **Yu T, Tsai J and Chang Y** (2018) A radial four-way power divider with the proposed isolation network. *IEEE Microwave and Wireless Components Letters* **28**, 194–196.
14. **Guo S, Song K, Zhou Y and Fan Y** (2018) Compact ultra-wideband bandpass-response power divider with high-frequency selectivity. *International Journal of Microwave and Wireless Technologies* **10**, 1107–1112.
15. **Song K, Mo Y, Xue Q and Fan Y** (2014) Wideband four-way out-of-phase slotline power dividers. *IEEE Transactions on Industrial Electronics* **61**, 3598–3606.
16. **Guo S, Song K and Fan Y** (2020) Compact four-way suspended-stripline power divider with low loss and high isolation. *International Journal of Microwave and Wireless Technologies* **12**, 1–5.
17. **Cano JL, Mediavilla A, Dragas S and Tazon A** (2016) Novel broadband circular waveguide four-way power divider for dual polarization applications. *IEEE Microwave & Wireless Components Letters* **26**, 98–100.
18. **Oraizi H and Ayati S-A.** Optimum design of a modified 3-way Bagley rectangular power divider," in *2010 10th Mediterranean Microwave Symposium*, pp. 25–28, IEEE, 2010/8/25 – 2010/8/27.
19. **Shan X and Shen Z** (2011) A suspended-substrate Ku-Band symmetric radial power combiner. *IEEE Microwave & Wireless Components Letters* **21**, 652–654.
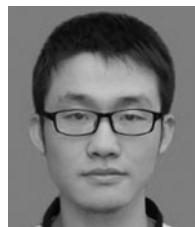
Song Guo was born in Lang Fang, Hebei Province, China, in February 1993. He received his B.Sc. degree in Microelectronics from Harbin Engineering University, Harbin, Heilongjiang, China, in 2006, and is currently working toward his M.Sc. degree in Electromagnetic Fields and Microwave Technology at the UESTC (University of Electronic Science and Technology of China). His research interests include microwave and millimeter-wave power-combining technology and microwave passive component design.

Kaijun Song received his M.S. degree in Radiophysics and a Ph.D. degree in Electromagnetic Field and Microwave Technology from the University of Electronic Science and Technology of China (UESTC), Chengdu, China, in 2005 and 2007, respectively. In 2011, he received the "New Century Excellent Talents in University Award" from the Chinese Ministry of Education. In 2015, he received the academic and technical leaders in Sichuan province. In 2019, he received the science and technology innovation talents in Sichuan province. Since 2007, he has been with the EHF Key Laboratory of Science, School of Electronic Engineering, UESTC, where he was a full professor. Since 2018, he is currently a full professor with the School of Electronic Science and Engineering, UESTC. From 2007 to 2008, he was a postdoctoral research fellow with the Montana Tech of the University of Montana, Butte, USA, working on microwave/millimeter-wave circuits and microwave remote sensing technologies. From 2008 to 2010, he was a research fellow with the State Key Laboratory of Millimeter Waves of China, Department of Electronic Engineering, City University of Hong Kong, on microwave/millimeter-wave power-combining technology and Ultra-Wideband (UWB) circuits. He was a senior visiting scholar with the State Key Laboratory of Millimeter Waves of China, Department of Electronic Engineering, the City University of Hong Kong, in November 2012. He has published more than 200 internationally refereed journal papers and conference papers. His current research fields include microwave and millimeter-wave/THz power-combining technologies, high-power solid-state microwave/millimeter-wave technologies, UWB circuits, and technologies; and microwave/millimeter-wave devices, circuits, and systems. Prof. Song is the Reviewer of tens of international journals, including IEEE Transactions and IEEE Papers.

Yong Fan (M'05) received a B.E. degree from Nanjing University of Science and Technology, Nanjing, Jiangsu, China, in 1985 and an M.S. degree from the University of Electronic Science Technology of China, Chengdu, Sichuan, China, in 1992. He is now with the School of Electronic Engineering, University of Electronic Science and Technology of China, where he is currently a full professor. His current research interests include electromagnetic theory, millimeter-wave technology, communication, and system. He has authored and co-authored over 130 papers. Mr. Fan is a senior member of the Chinese Institute of Electronics.